List of Supplementary Tables and Figures

Figure S10. Domain average summer and winter diurnal cycles of LU-specific O_3 inverted in-canopy convective resistances for M3DRY_2016 and STAGE_2016.

Figure S11. Domain average summer and winter diurnal cycles of LU-specific O_3 inverted canopy quasi-laminar sublayer resistances for M3DRY_2016 and STAGE_2016. Note that in M3Dry, the quasi-laminar sublayer resistance is pathway independent while in STAGE it differs between the canopy (cuticular and stomatal) and ground (vegetated and bare soil) pathways.

Figure S12. Domain average summer and winter diurnal cycles of LU-specific O_3 inverted ground quasi-laminar sublayer resistances for M3DRY_2016 and STAGE_2016. Note that in M3Dry, the quasi-laminar sublayer resistance is pathway independent while in STAGE it differs between the canopy (cuticular and stomatal) and ground (vegetated and bare soil) pathways.

Figure S13. Domain average summer and winter diurnal cycles of LU-specific O_3 inverted aerodynamic resistances for M3DRY_2016 and STAGE_2016.

Figure S14. Left column: annual mean WRF PX grid-scale (top row) and LU-weighted sum of LU-specific u_* values for M3DRY_2016 (second row), STAGE_2016 (third row), and STAGE_REF_2016 (fourth row). Center column: absolute differences between annual mean LU-weighted sum of LU-specific and WRF PX grid-scale u_* values. Right columns: percentage differences between annual mean LU-weighted sum of LU-specific and WRF PX grid-scale u_* values.

Figure S15. Left column: annual mean WRF PX grid-scale (top row) and LU-weighted sum of LU-specific inverted R_a values for M3DRY_2016 (second row), STAGE_2016 (third row), and STAGE_REF_2016 (fourth row). Center column: absolute differences between annual mean LU-weighted sum of LU-specific and WRF PX grid-scale inverted R_a values. Right columns: percentage differences between annual mean LU-weighted sum of LU-specific and WRF PX grid-scale inverted R_a values.

Figure S16: Maps of differences in the fractional coverage of the 16 AQMEII4 LU categories (Galmarini et al., 2021) between the M3Dry simulations using WRF PX LSM configured with MODIS and NLCD LU (i.e. M3DRY_2016 and M3DRY_NLCD40_2016), respectively. Differences are shown as M3DRY_2016 - M3DRY_NLCD40_2016. As noted in Section 2.3.1, the CMAQ M3Dry calculations and post-processor estimates of LU specific and aggregated diagnostic variables were performed using native LU categories from the MODIS and NLCD schemes. Aggregation to the 16 category AQMEII4 LU scheme was performed through mapping and LU weighted averaging of equivalent categories (Table S1). None of the MODIS LU categories correspond to the AQMEII4 herbaceous category.

Table S1: Mapping of MODIS and NLCD LU categories to AQMEII4 LU categories (see Sections 2.3.1 and 2.3.2 for further details on different approaches between M3Dry and STAGE)

AQMEII4 LU Category	MODIS LU Category	NLCD LU Category
1: Water	17: Water	17: Water
2: Developed / Urban	13: Urban and Built-up	13: Urban and Built-up
		23: Developed open space
		24: Developed Low Intensity
		25: Developed Medium Intensity
		26: Developed High Intensity
3: Barren	16: Barren or Sparsely Vegetated	16: Barren or Sparsely Vegetated
		27: Barren Land
4: Evergreen needleleaf forest	1: Evergreen Needleleaf Forest	1: Evergreen Needleleaf Forest
		29: Evergreen Forest
5: Deciduous needleleaf forest	3: Deciduous Needleleaf Forest	3: Deciduous Needleleaf Forest
6: Evergreen broadleaf forest	2: Evergreen Broadleaf Forest	2: Evergreen Broadleaf Forest
7: Deciduous broadleaf forest	4: Deciduous Broadleaf Forest	4: Deciduous Broadleaf Forest
		28: Deciduous Forest
8: Mixed forest	5: Mixed Forest	5: Mixed Forest
		30: Mixed Forest
9: Shrubland	6: Closed Shrublands	6: Closed Shrublands
	7: Open Shrublands	7: Open Shrublands
		32: Shrub/Scrub
10: Herbaceous		34: Sedge/Herbaceous (not present in domain)
11: Planted/Cultivated	12: Croplands	12: Croplands
	14: Cropland-Natural Vegetation Mosaic	14: Cropland-Natural Vegetation Mosaic
		37: Pasture/Hay
		38: Cultivated Crops
12: Grassland	10: Grasslands	10: Grasslands
		33: Grassland/Herbaceous
13: Savanna	8: Woody Savanna	8: Woody Savanna
	9: Savanna	9: Savanna
14: Wetlands	11: Permanent Wetlands	11: Permanent Wetlands
		39: Woody Wetland
		40: Emergent Herbaceous Wetland
15: Tundra	18: Wooded Tundra	31: Dwarf Scrub (not present in domain)
	19: Mixed Tundra	35: Lichens (not present in domain)
	20: Barren Tundra (not present in domain)	36: Moss (not present in domain)
16: Snow and Ice	15: Snow and Ice	15: Snow and Ice
		22: Perennial Ice/snow (not present in domain)

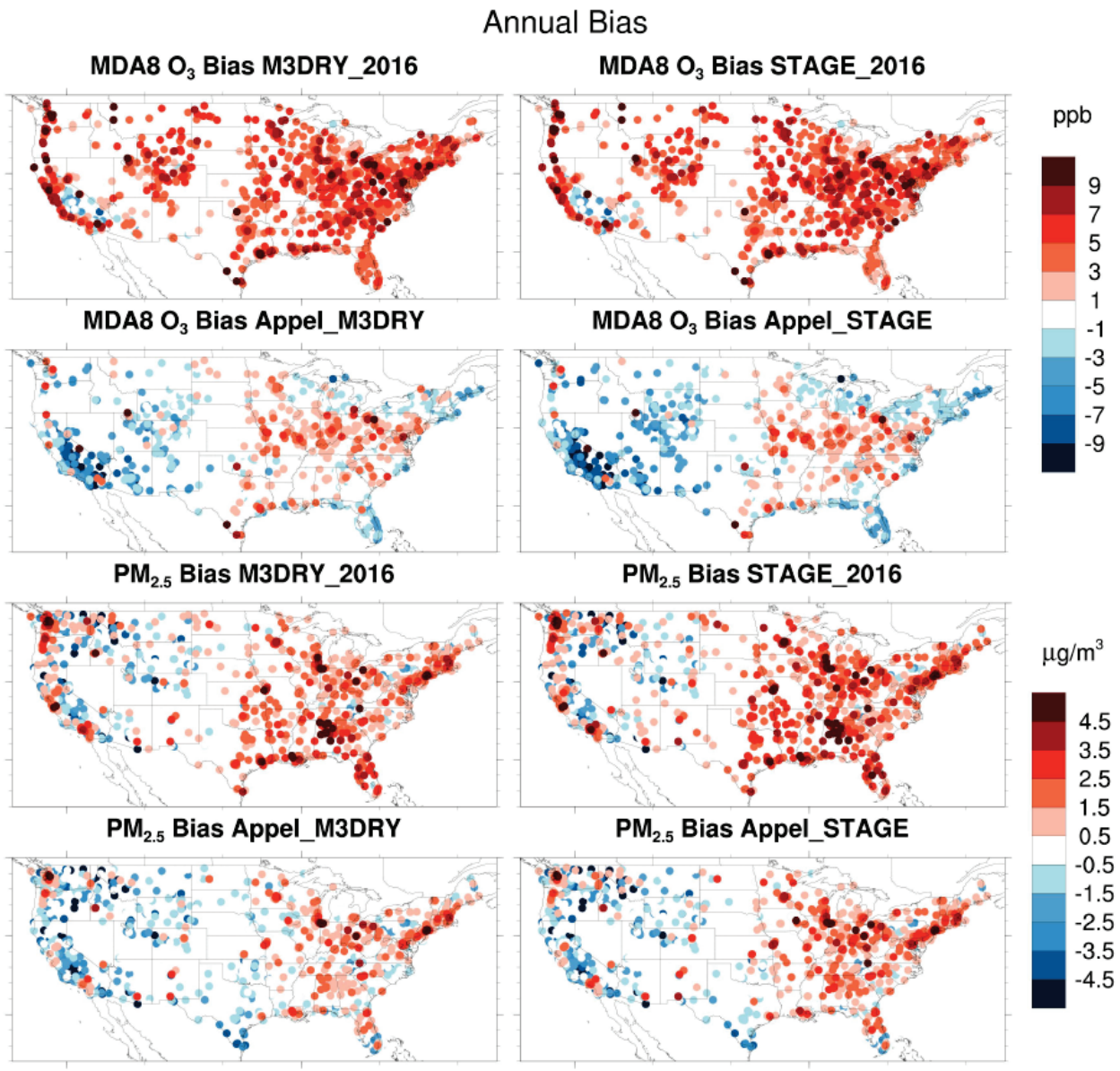

Figure S1: Annual MDA8 O_3 and $PM_{2.5}$ mean biases for the M3DRY_2016 and STAGE_2016 base case simulations analyzed in this study this study and the corresponding "CMAQ531_WRF411_M3Dry_BiDi" and "CMAQ531_WRF411_STAGE_BiDi" 2016 CMAQv5.3.1 simulations analyzed in Appel et al. (2021).

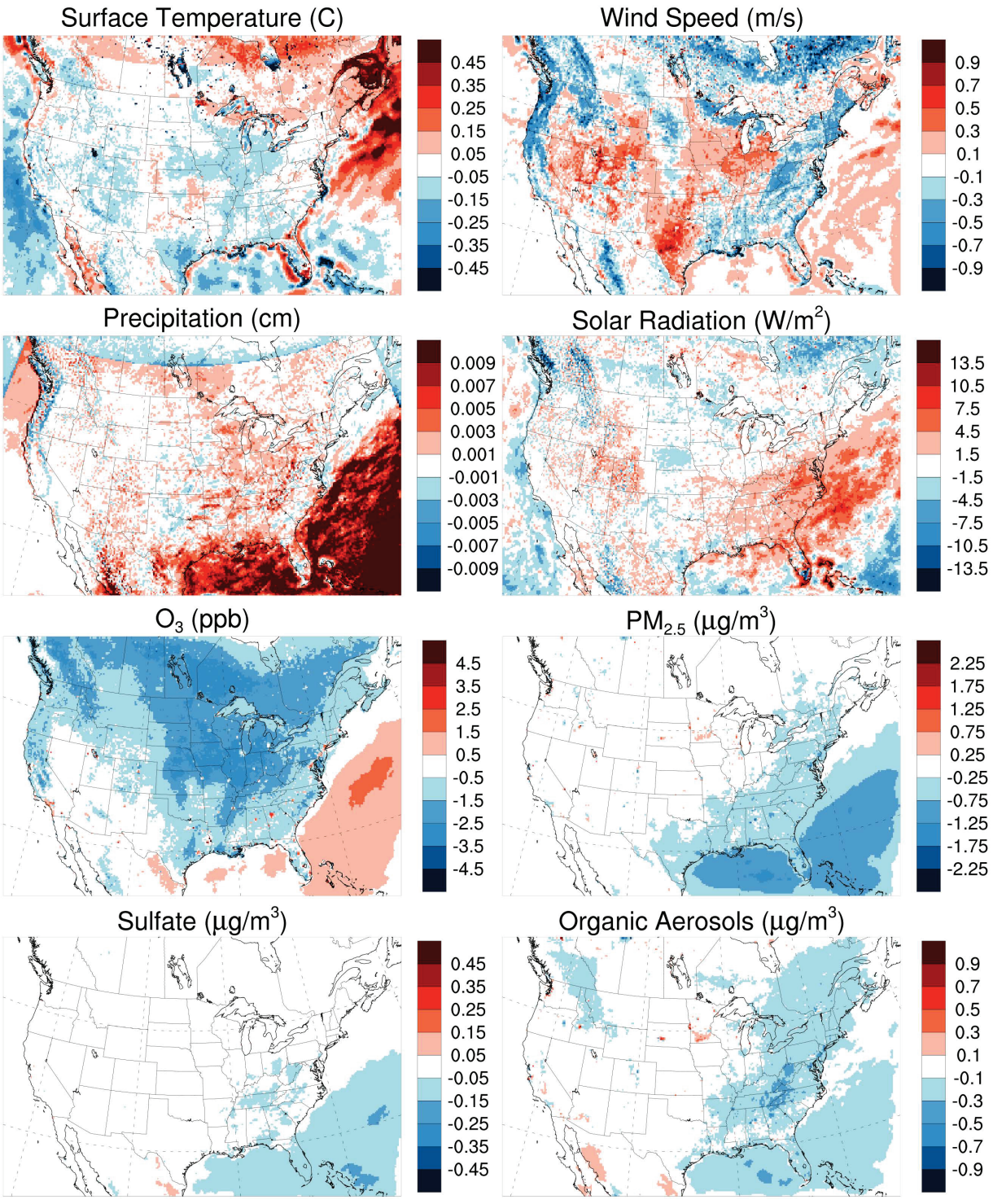

Figure S2: Impact of different WRF configuration options used in this study vs. Appel et al. (2021) on annual mean surface values of several meteorological fields, O_3, and aerosol species. The maps show absolute differences calculated as M3DRY_2016 minus M3DRY_LTNGNO_BASE_2016.

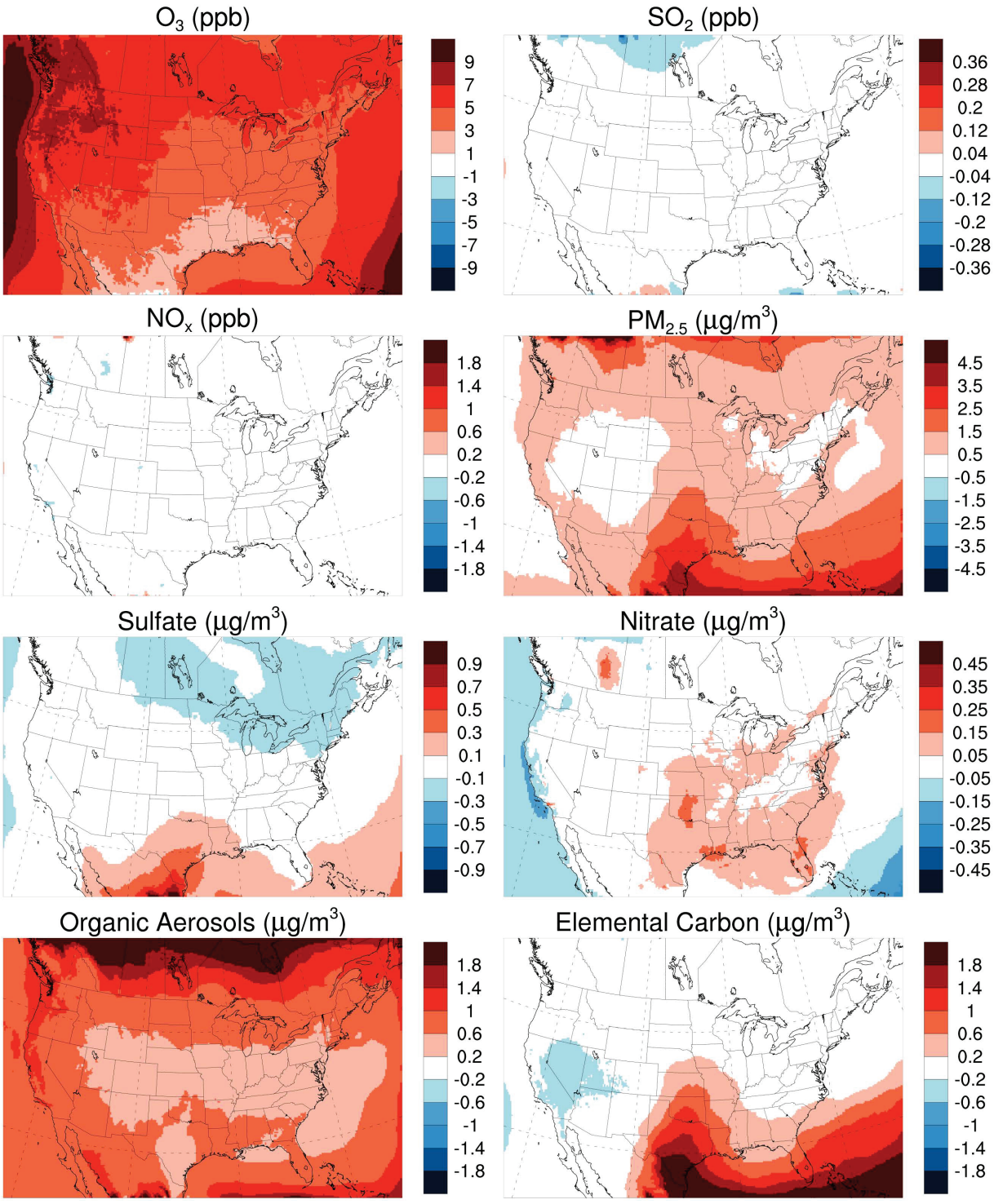

Figure S3: Impact of different lateral boundary conditions used in this study vs. Appel et al. (2021) on annual mean surface values of several gas phase and aerosol species. The maps show absolute differences calculated as M3DRY_2016 minus M3DRY_HCMAQ_2016.

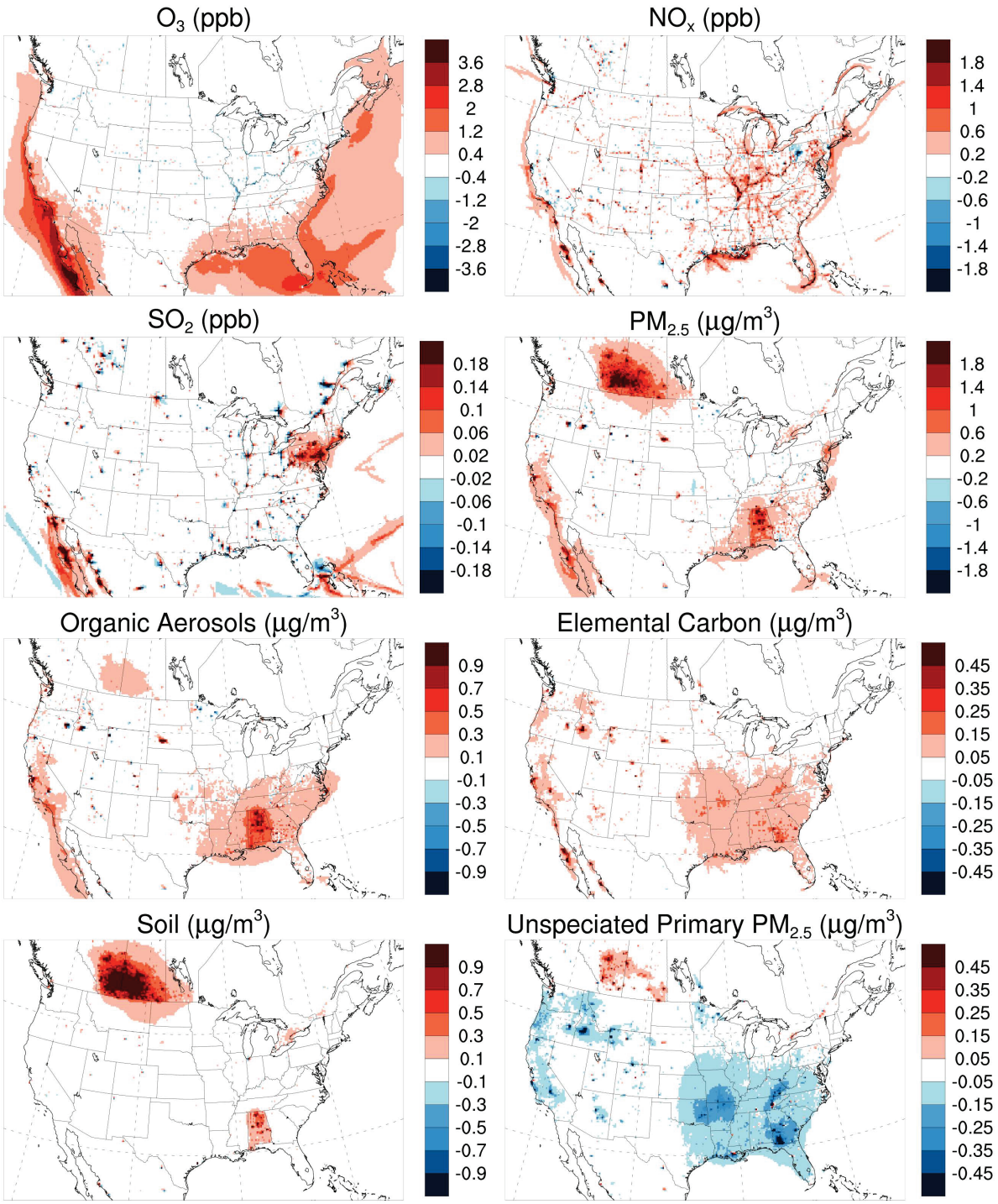

Figure S4: Impact of different anthropogenic and fire emission files used in this study vs. Appel et al. (2021) on annual mean surface values of several gas phase and aerosol species. The maps show absolute differences calculated as M3DRY_2016 minus M3DRY_APPEL_EMIS_2016. “Soil” fine aerosol concentrations are estimated from simulated crustal elements as 2.20*Al + 2.49*Si + 1.63*Ca + 2.42*Fe + 1.94*Ti.

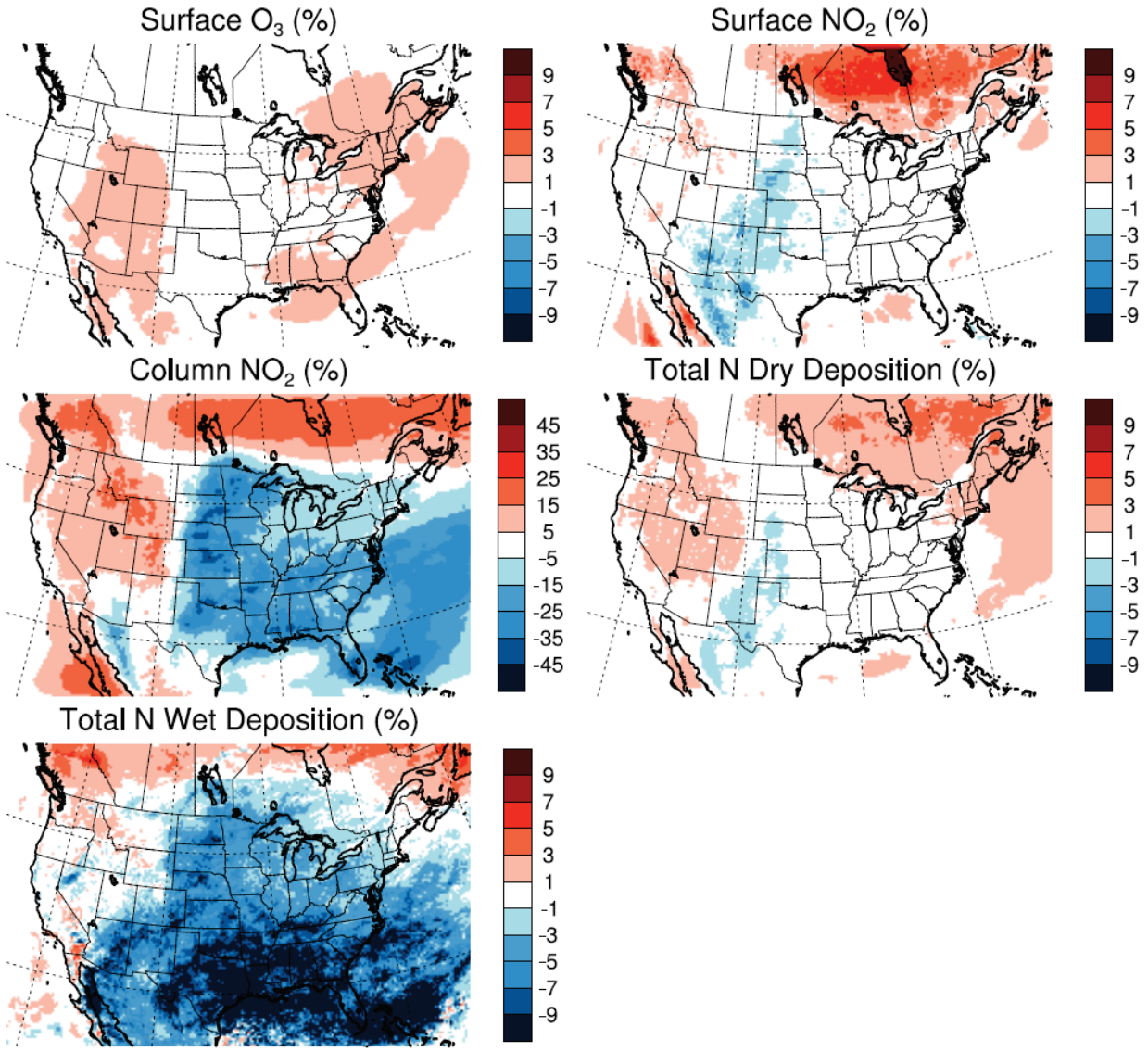

Figure S5: Impact of different lightning NO emission representation on May – September surface mixing ratios of O_3 and NO_2, column NO_2, and dry and wet deposition of total nitrogen. The maps show percentage differences calculated as M3DRY_LTNGNO_BASE_2016 minus M3DRY_LTNGNO_NLDN_2016 relative to M3DRY_LTNGNO_BASE_2016.

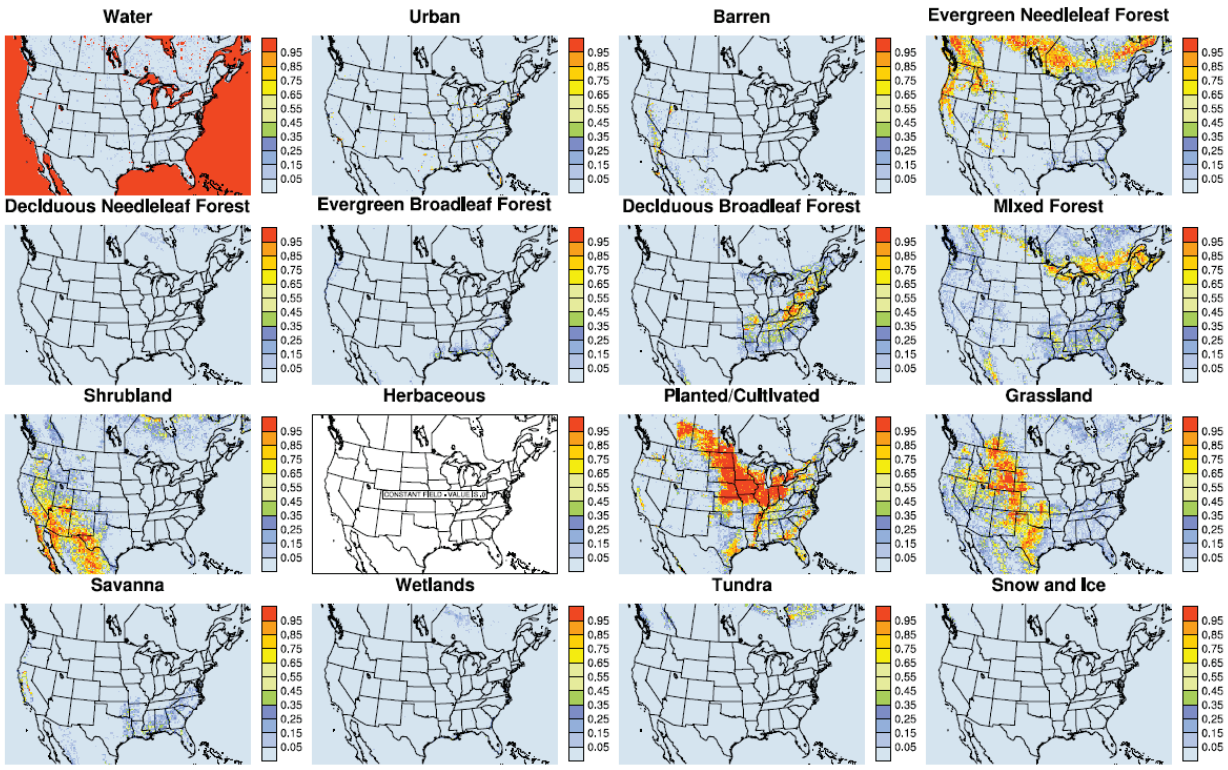

Figure S6: Maps of fractional coverage of the 16 AQMEII4 LU categories (Galmarini et al., 2021) in the M3DRY_2016 simulations using MODIS LU. As noted in Section 2.3.1, the M3Dry simulations were performed using the 20 native MODIS LU categories and the mapping to the AQMEII4 categories was performed during post-processing. None of the 20 MODIS LU categories correspond to the AQMEII4 herbaceous category.

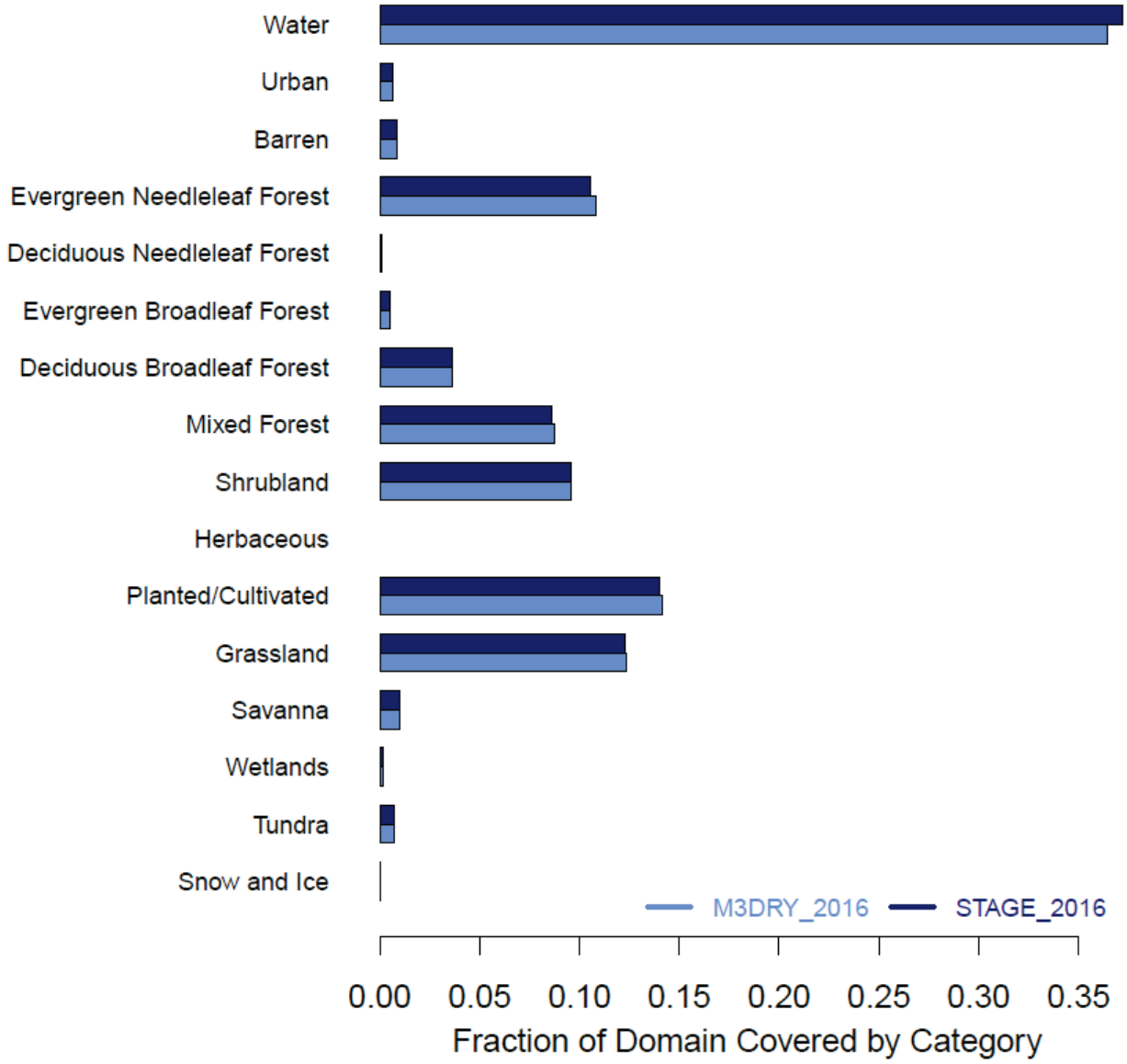

Figure S7: Domainwide fractional coverage of the 16 AQMEII4 LU categories (Galmarini et al., 2021) in the M3DRY_2016 and STAGE_2016 simulations. As noted in Section 2.3.1, the M3Dry simulations were performed using the 20 native MODIS LU categories and the mapping to the AQMEII4 categories was performed during post-processing while the STAGE simulations were performed using the AQMEII4 categories. None of the 20 MODIS LU categories correspond to the AQMEII4 herbaceous category. See discussion in the text on the small differences in fractional coverage between M3DRY_2016 and STAGE_2016.

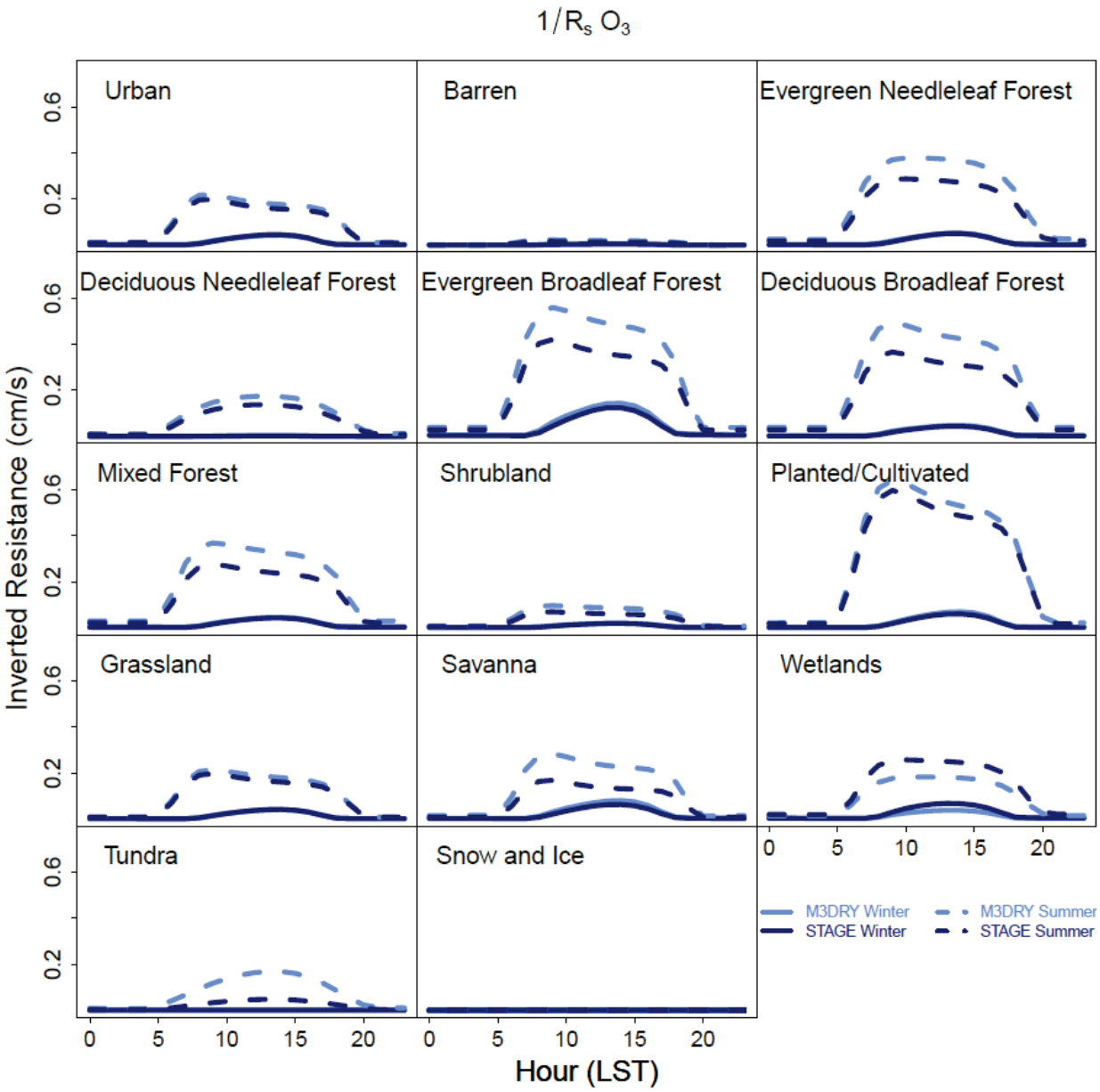

Figure S8. Domain average summer and winter diurnal cycles of LU-specific O_3 inverted stomatal resistances for M3DRY_2016 and STAGE_2016.

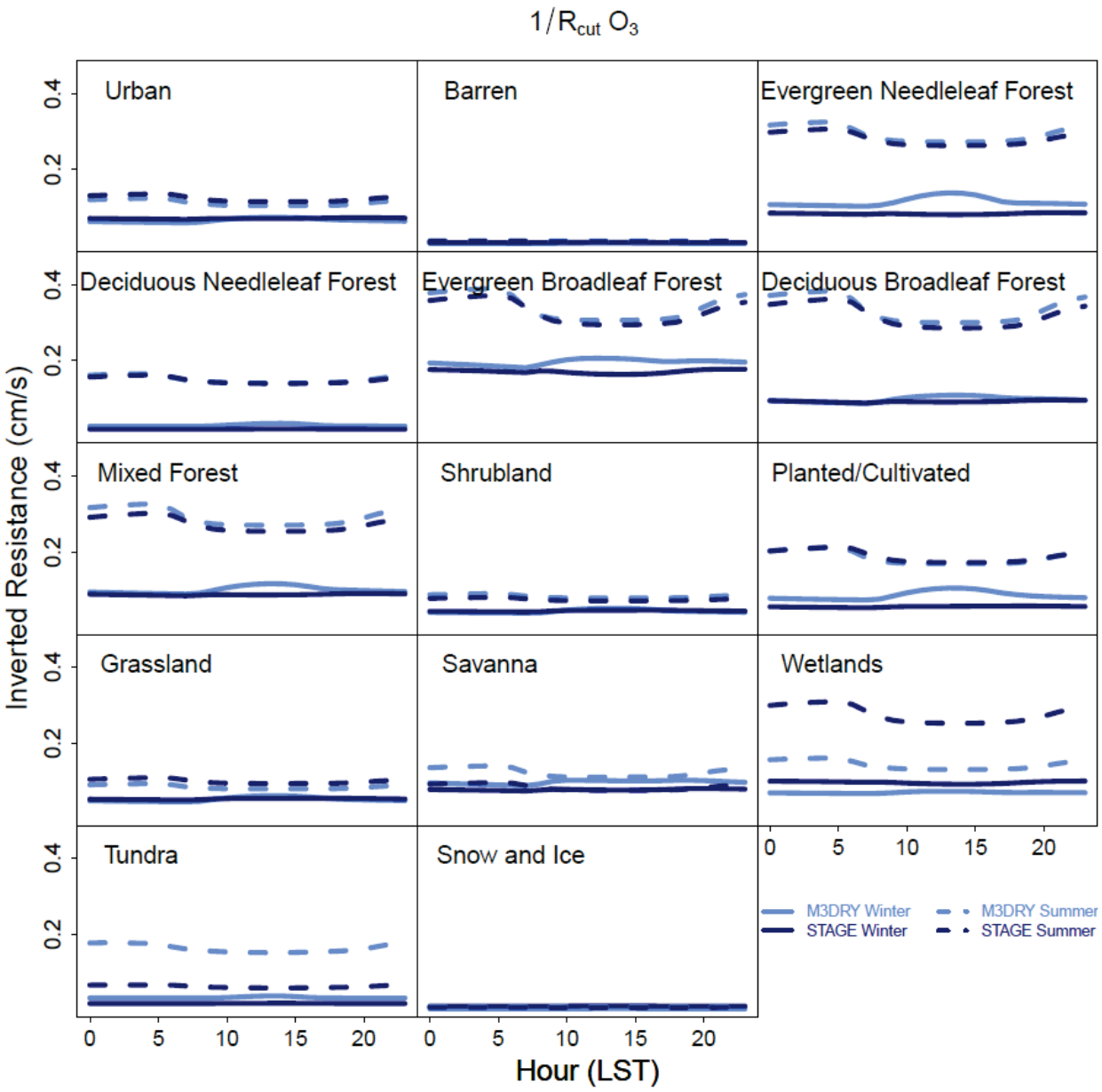

Figure S9. Domain average summer and winter diurnal cycles of LU-specific O_3 inverted cuticular resistances for M3DRY_2016 and STAGE_2016.

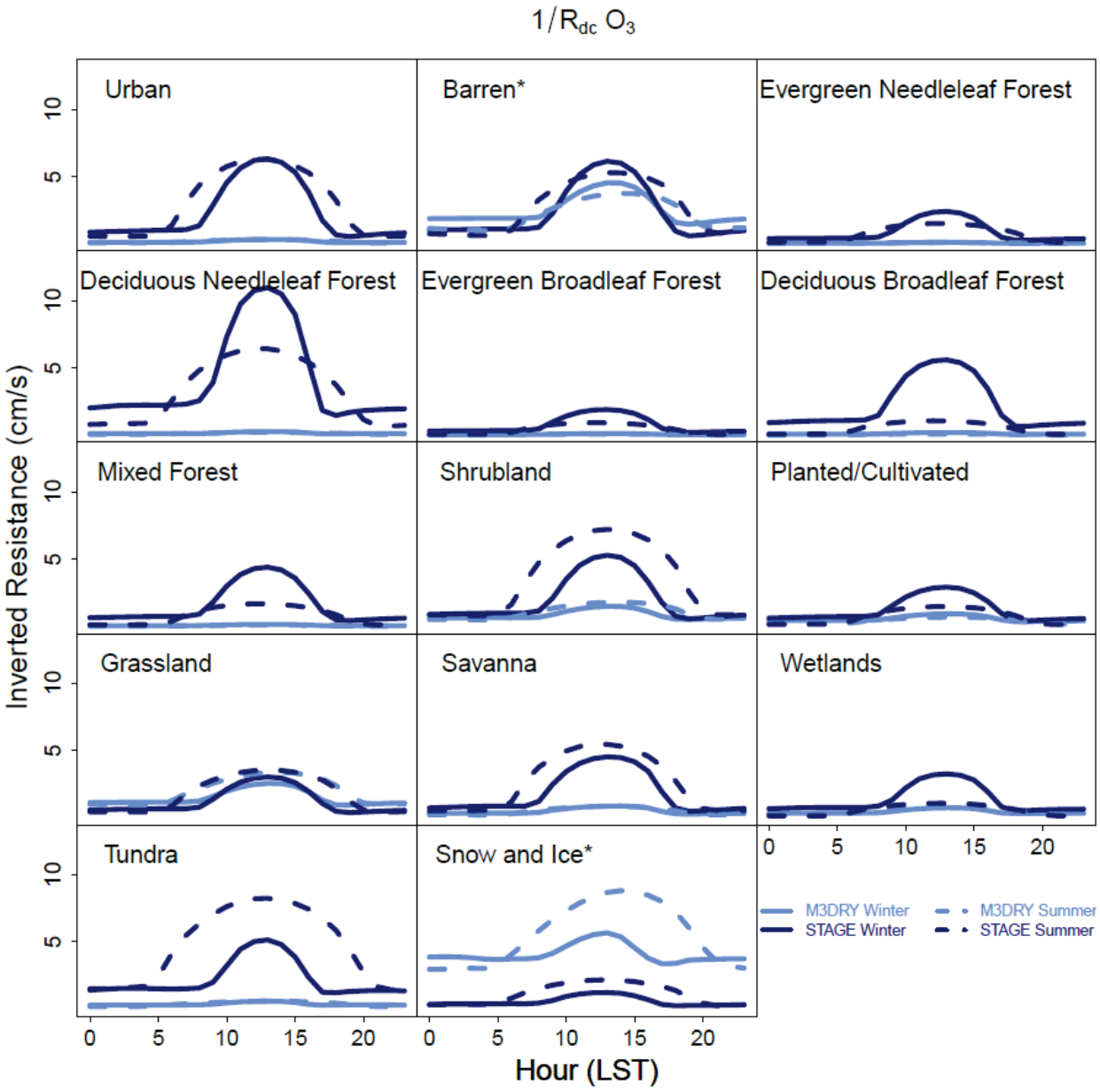

Figure S10. Domain average summer and winter diurnal cycles of LU-specific O_3 inverted in-canopy convective resistances for M3DRY_2016 and STAGE_2016.

*Values for the barren and snow and ice LU categories were divided by 10 and 30, respectively, to fit on the same y-axis as values for all other LU categories

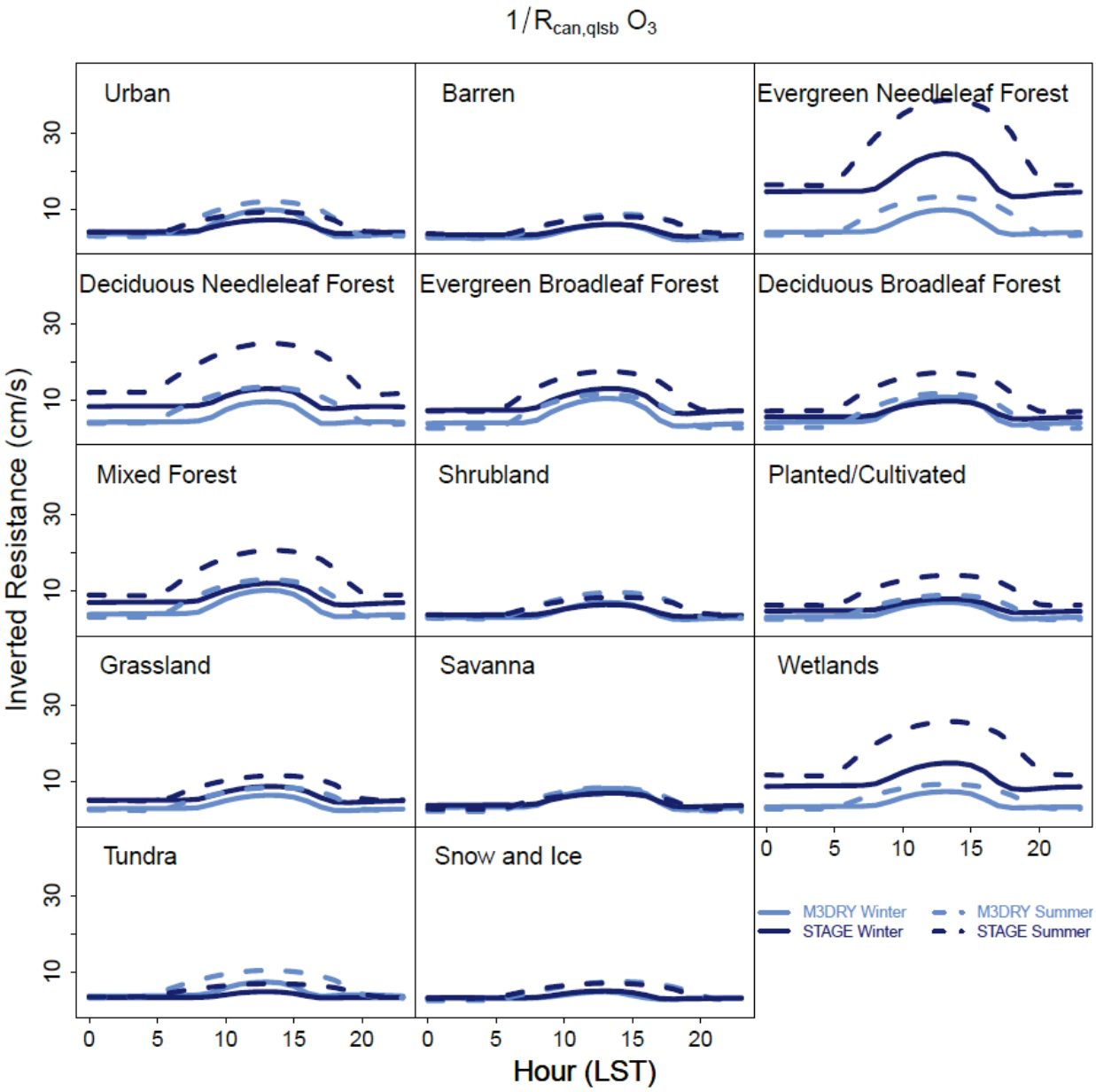

Figure S11. Domain average summer and winter diurnal cycles of LU-specific O_3 inverted canopy quasi-laminar sublayer resistances for M3DRY_2016 and STAGE_2016. Note that in M3Dry, the quasi-laminar sublayer resistance is pathway independent while in STAGE it differs between the canopy (cuticular and stomatal) and ground (vegetated and bare soil) pathways.

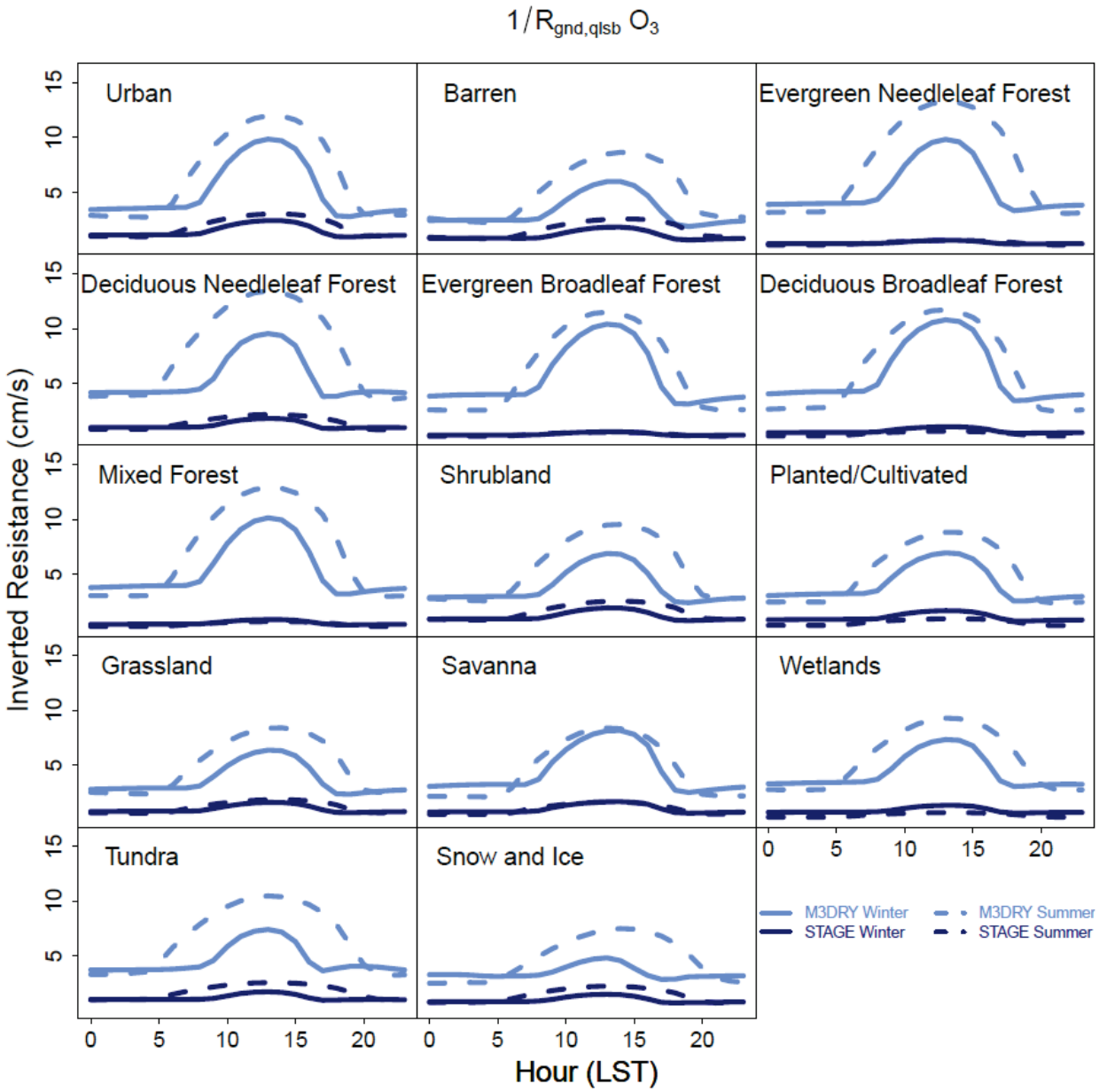

Figure S12. Domain average summer and winter diurnal cycles of LU-specific O_3 inverted ground quasi-laminar sublayer resistances for M3DRY_2016 and STAGE_2016. Note that in M3Dry, the quasi-laminar sublayer resistance is pathway independent while in STAGE it differs between the canopy (cuticular and stomatal) and ground (vegetated and bare soil) pathways.

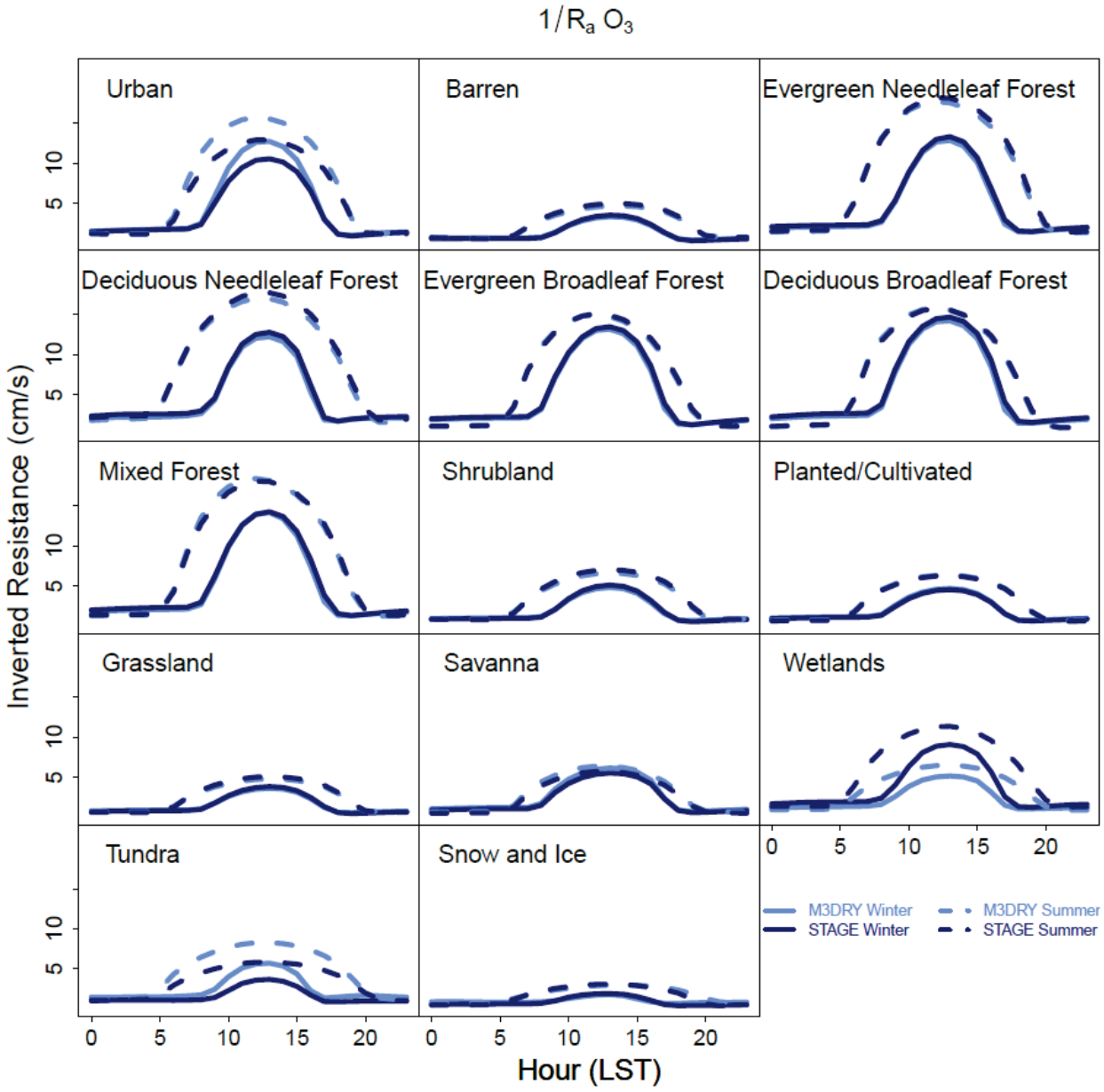

Figure S13. Domain average summer and winter diurnal cycles of LU-specific O_3 inverted aerodynamic resistances for M3DRY_2016 and STAGE_2016.

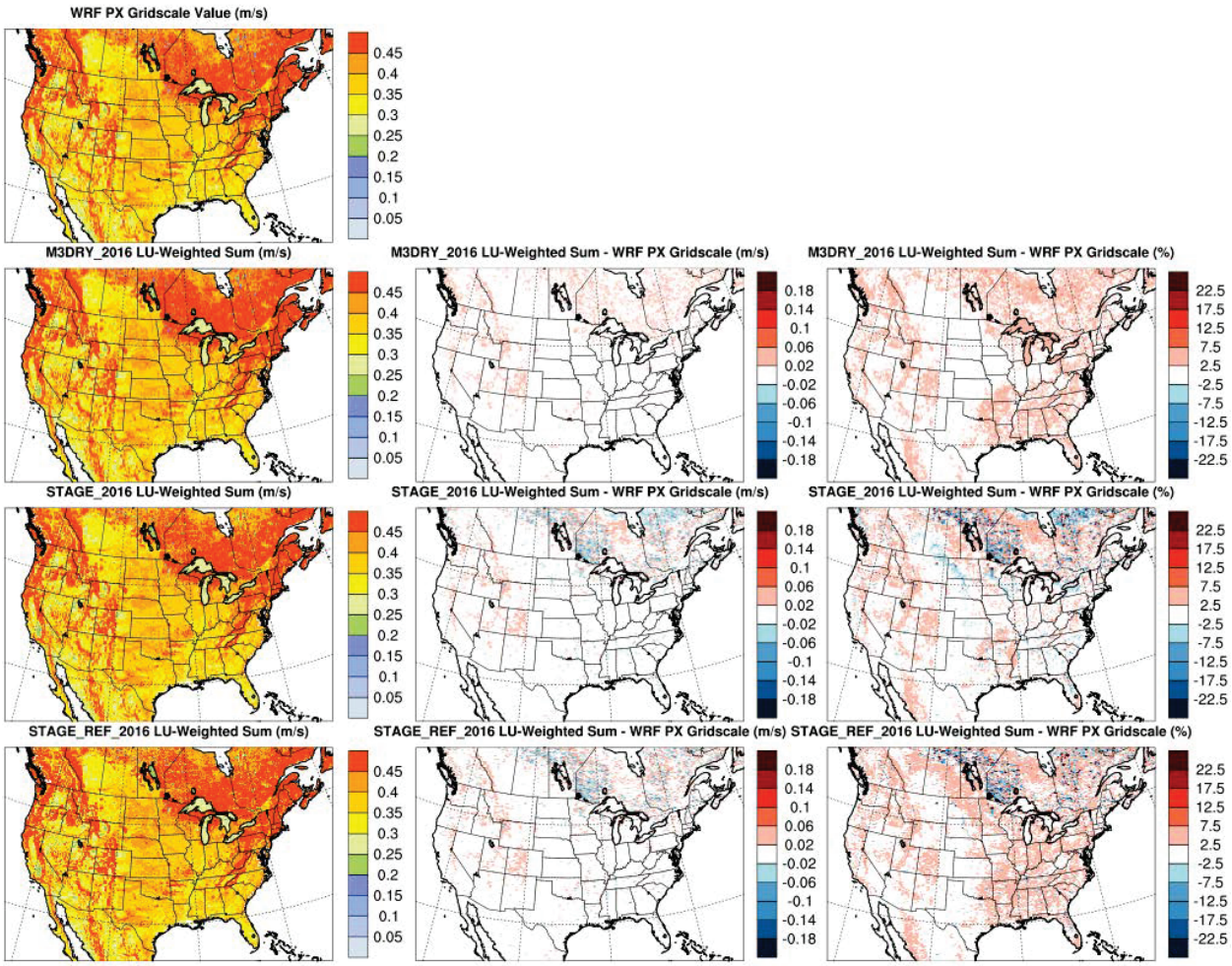

Figure S14. Left column: annual mean WRF PX grid-scale (top row) and LU-weighted sum of LU-specific u_* values for M3DRY_2016 (second row), STAGE_2016 (third row), and STAGE_REF_2016 (fourth row). Center column: absolute differences between annual mean LU-weighted sum of LU-specific and WRF PX grid-scale u_* values. Right columns: percentage differences between annual mean LU-weighted sum of LU-specific and WRF PX grid-scale u_* values.

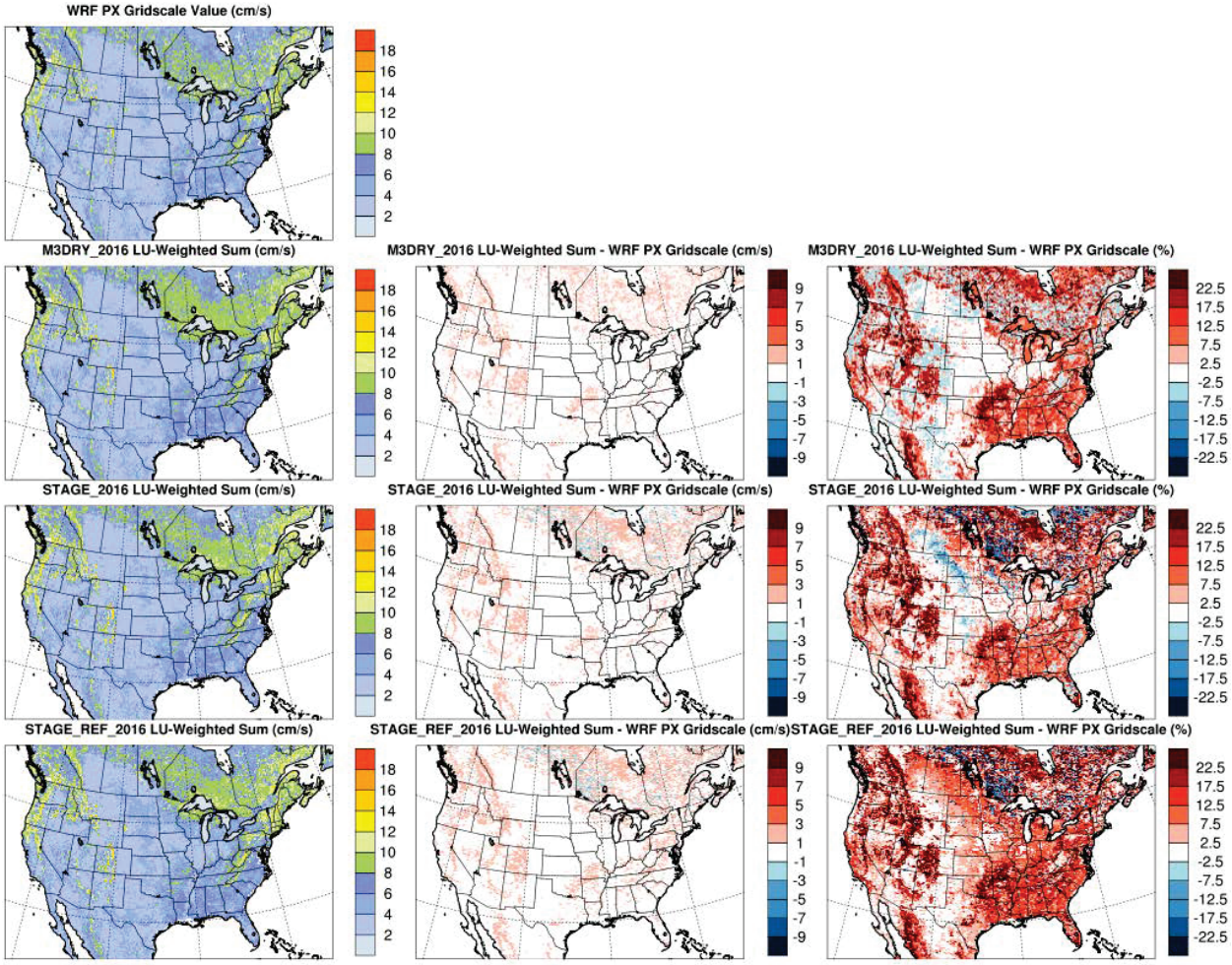

Figure S15. Left column: annual mean WRF PX grid-scale (top row) and LU-weighted sum of LU-specific inverted R_a values for M3DRY_2016 (second row), STAGE_2016 (third row), and STAGE_REF_2016 (fourth row). Center column: absolute differences between annual mean LU-weighted sum of LU-specific and WRF PX grid-scale inverted R_a values. Right columns: percentage differences between annual mean LU-weighted sum of LU-specific and WRF PX grid-scale inverted R_a values.

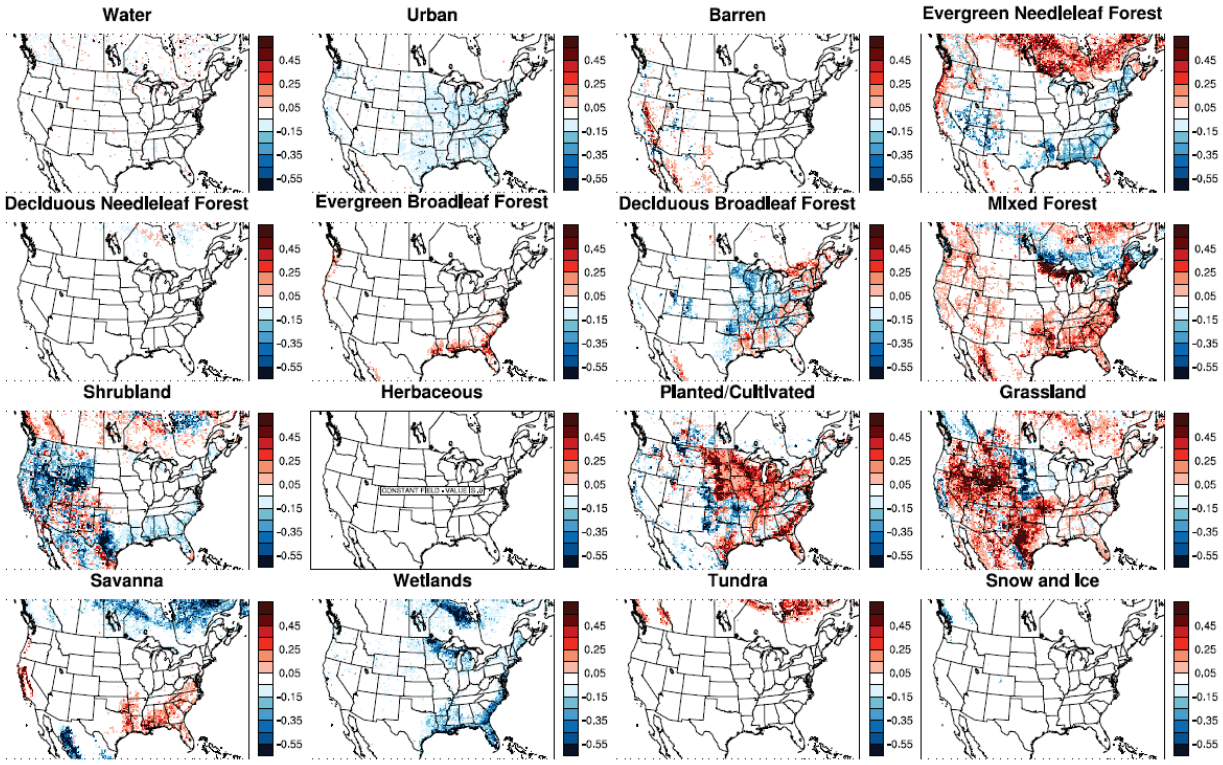

Figure S16: Maps of differences in the fractional coverage of the 16 AQMEII4 LU categories (Galmarini et al., 2021) between the M3Dry simulations using WRF PX LSM configured with MODIS and NLCD LU (i.e. M3DRY_2016 and M3DRY_NLCD40_2016), respectively. Differences are shown as M3DRY_2016 - M3DRY_NLCD40_2016. As noted in Section 2.3.1, the CMAQ M3Dry calculations and post-processor estimates of LU specific and aggregated diagnostic variables were performed using native LU categories from the MODIS and NLCD schemes. Aggregation to the 16 category AQMEII4 LU scheme was performed through mapping and LU weighted averaging of equivalent categories (Table S1). None of the MODIS LU categories correspond to the AQMEII4 herbaceous category.